# Microbial membrane reordering in response to butanol: interdigitation *vs* disorder

Jingjing Guo, James Ho C.S., Hokyun Chin, Jamie Hinks, Alan E. Mark, Cheng Zhou, Staffan Kjelleberg, Bo Liedberg, Atul Parikh, Yuguang Mu & Thomas Seviour

While lipid bilayer perturbation is a major toxicity determinant of butanol limiting the financial competitiveness of bio-butanol production, the underlying mechanisms remain~~s~~ unclear. Here, we reveal the effects of butanol on a representative *Escherichia coli* inner membrane by combining computational and experimental approaches. A critical maximum butanol:lipid ratio for bilayer stability of 2:1 was observed in our simulations, consistent with the fully interdigitated state. However, the thickness of the sub-critical butanol-treated bilayer was ~20% greater than in a fully interdigitated one. Additionally, butanol intercalation was accompanied by acyl chain bending and increased disorder, which are inconsistent with the interdigitated gel state. Our simulations thus suggest that butanol induces only partial interdigitation of *E. coli* membranes at physiological temperatures. This is due to non-uniform accumulation of butanol with the phospholipid heads, which creates voids that are predominately filled by increased disorder (i.e. splaying and bending of acyl tails within the same leaflet). Finally, butanol short-circuits the lipid bilayer and creates a coupled system where interdigitated and splayed phospholipids coexist. Experimental measurements were carried out to complement our modelling observations. Resolving the effects of butanol on a bacterial membrane will help us understand natural adaptations for enhanced butanol tolerance and inform the design of new strategies targeting membrane bilayer stability for increasing biobutanol production titres.

## Introduction

Butanol is attractive as both as an advanced fuel or platform chemical. It has a higher energy density, lower hygroscopicity and lower vapor pressure than ethanol, and is more compatible with existing transportation infrastructure. Fermentation is potentially the most sustainable source of butanol (i.e. bio-butanol) relative to petrochemical. Several microbes have been considered for bio-butanol production, including genetically engineered *E. coli*[1]. However, butanol toxicity currently remains a barrier to achieving sufficiently high production titres. At butanol concentrations of 1% (*v/v*), wild type *E. coli* growth is almost completely inhibited, while some butanol-tolerant *E. coli* strains can only can tolerate up to 1.5% (*v/v*) butanol[1-3]. At high concentrations, butanol increases membrane fluidity causing cell leakage[4], impairs internal pH regulation, inhibits glucose uptake[5], and ultimately kills cells[6].

Butanol partitioning into cytoplasmic membranes increases membrane fluidity by disrupting membrane integrity, which is a major toxicity determinant of butanol. It was found that cells can adapt to butanol by modifying their lipid composition. For example, by increasing the ratio of saturated to unsaturated acyl chains[7, 8], it is hypothesised to compensate for the increase in cell membrane fluidity. Therefore, maintaining inner membrane stability in the presence of butanol is a critical aspect of minimising butanol toxicity and enabling efficient large-scale bio-butanol production.

Elucidating exactly how butanol interferes with bacterial membranes, particularly under physiologically relevant conditions, is confounded by the fact that bilayers can exist in either fluid or gel state, as well as the purported existence of an ordered interdigitated state. Interdigitation contradicts descriptions of increased membrane fluidity, which would be consistent with a more disordered state. Cell membranes are fluid at physiological temperatures, while at lower temperatures, they become gel-like. The assimilation of alcohols at the bilayer/water surface is thought to introduce voids in the hydrophobic core, which is an energetically unfavorable condition. It has been suggested that when in the gel phase, in order to achieve a low energy state, the acyl chains from the opposing leaflet can fill this void leading to an ordered and interdigitated gel state[9-14]. Thus, each phospholipid would be shielded from water through aligning with a pair of alcohols in the opposing leaflet. This has been used to explain the increase by ethanol in bilayer molecular order in the gel and ripple phases, and the associated reduction in lipid mobility[15]. Accordingly, membrane thickness was found to be reduced by ethanol to the sum of the length of the hydrophobic tails of phospholipids and the alcohols.

Further complicating attempts to resolve the effect of butanol on phospholipid bilayers are findings that alcohols with different chain lengths have opposing effects, suggesting that in fact multiple factors might be involved in the disruption of phospholipid bilayers by alcohols. Alcohols only up to chain lengths of seven carbons (i.e. not octanol or nonanol), including

branched ones, have been shown to induce interdigitation in a bilayer composed of saturated phospholipids, but only when in the gel phase[13, 14]. In contrast, in the fluid phase the membranes were found to become more disordered. Following short-chain alcohol exposure, ~~membrane~~ membrane expansion, disorder and the extent of lipid acyl chain interdigitation increased while membrane thickness was reduced[16-18]. Exposure to long-chain alkanols, on the other hand, had the opposite effects[17], i.e. higher order, and melting temperature (Tm), with the exceptions that bilayer thickness was increased and area per lipid was decreased. Interestingly, in certain cases, monounsaturated phospholipids have also been shown to adopt an interdigitated state[19, 20]. Hence, short-chain and long-chain alcohols appear to have distinct modes of interactions with lipid membranes.

We hypothesized that, while not necessarily measurable as a bulk biophysical property, multiple factors likely contribute to the net effect of butanol on a bacterial phospholipid bilayer under physiological conditions. The aim of the present study was therefore to elucidate, at a molecular and atomic scale, the various ways in which butanol contributes to bilayer reordering.

Computational modelling is one of the best strategies for resolving intermolecular interactions at an atomic level. It can provide structural information otherwise unattainable by experiments and has been applied to study cell membranes to address questions such as how membranes respond to small organic molecules[21-25], are stabilized by insertion molecules[26], and permeabilized by alcohols[27]. Although several computational studies have been performed on the effect of butanol of the cytoplasmic bilayer, most have relied on coarse-graining models and do not use bacteria relevant phospholipids[28-31]. A systematic molecular level description of butanol-challenged *E. coli* membranes is still missing. Herein extensive molecular dynamics simulations were performed on an 85:15 phosphatidylethanolamine:phosphatidylglycerol (POPE:POPG) bilayer, which more accurately represents the inner membrane of *E. coli*[32], attempting to understand the relationship between interdigitation and intrinsic disorder in a butanol-treated bilayer. Additionally, experimental measurements were carried out to complement our modelling observations, providing a unifying molecular mechanism underlying the membrane perturbing effects of butanol. Such resolution is required to rationally engineer bilayers for enhanced butanol tolerance, which will enable increased production titres and promote the viability of industrial biobutanol production.

## Results and discussion

### Partitioning of butanol into membrane reduces gel-to-liquid-crystalline main transition temperature

To obtain an initial understanding of the effects of butanol on the POPE:POPG lipid bilayer system, we performed differential scanning calorimetry (DSC) measurement using large unilamellar vesicles (LUVs) dosed with butanol (0-4 *v/v*%). The heating and cooling scans were repeated three times and the thermograms were fully reproducible. A single exothermic peak with a maximum of 22.11˚C was detected in the differential scanning calorimetry heating curve (Fig 1,S1a), indicating a gel-to-liquid-crystalline transition ($T_m$) of the POPE:POPG lipid bilayer that is consistent with values obtained for similar compositions[33]. A monophasic reduction in the $T_m$ of the LUVs from 20.88˚C to 12.18˚C was observed in the heating scan as butanol concentrations were raised from 0.25-4.00%v/v (Fig 1,S1a,c). While a $T_m$ hysteresis of -1.96˚C was determined from the cooling scan for the LUVs without butanol (Fig 1, S1b,c), this increased from -2.13 to -3.12˚C as the butanol concentration was increased.

A bilayer undergoing inter-digitation would be expected to display biphasic behaviour for $T_m$, pre-transition peak suppression and increased $T_m$ hysteresis in the calorimetric response. However, here we observed a monophasic decreasing trend and no pre-transition peak. Furthermore, $\Delta T_{1/2}$ (8 ±11 % change) for the main transition peak (i.e. full width at half maximum) and $\Delta H$ (8 ±5 % change) were similar for all butanol concentrations compared to control, suggesting that the nature of the acyl chain interaction did not change with increasing butanol concentration.

The weakening of tail-tail Van der Waals attraction, suggested by the decrease in $T_m$ when butanol was mixed with LUVs, is likely due to the direct effect of inserting butanol into the interfacial area. The PE:PG headgroup interaction is also important to mitigate the destabilizing effect of the PG headgroup (i.e. negative at pH 7.5) on the bilayer. Thus, butanol insertion may also indirectly undermine bilayer stability by interfering with this headgroup packing to weaken the PE:PG interaction[34]. This intercalation of butanol likely causes an increase in the lateral spacing between adjacent phospholipids to create voids within the acyl chains, allowing more butanol to become incorporated within the bilayer.

**A critical butanol:lipid ratio of 2:1 is observed**

To provide an explanation for this behavior at the atomic scale, we undertook molecular dynamics simulations on three separate PE:PG bilayers, which were exposed to increasing bulk butanol concentrations (1.8, 3.6 and 5.4 *v/v* % respectively, designated as BOL1, BOL2 and BOL3) (Fig. 2a). Equilibrium was reached when the amount of butanol intercalating the bilayer (i.e. the ratio of butanol to phospholipid) and the bulk phase butanol concentration became constant. In all simulations, equilibrium was reached within 20 ns of adding butanol to the bulk phase (Fig. S2b and S2c). Butanol was found to deplete rapidly from the bulk phase as it partitioned into the bilayer (Fig. S2). This is not representative of what takes place in actual systems, where mass transfer of butanol from the bulk to the cell interface still maintains high butanol concentrations at the cell-liquid interface. To accurately describe butanol-bilayer interaction and correct for the depleting bulk butanol within a single simulation run, a number of sequential iterations were performed, whereby "new" butanol molecules were replenished into the system following the partitioning of "old" butanol into the bilayer, to maintain certain bulk concentrations (Fig. 2a, Table 1). For instance, BOL3-5 refers to the $5^{th}$ iteration for BOL3 system. We observed that the fraction of butanol molecules partitioning into the bilayer decreased with each iteration with increasing butanol concentration, as illustrated by the BOL3 simulations (Fig. 2b), suggesting a reduction in the partition coefficient of butanol from the bulk phase to the bilayer as the bilayer becomes increasingly saturated with butanol.

The intercalation of butanol into the membrane was accompanied by a marked lateral expansion in the membrane, with a ~40% increase in area per lipid headgroup from an average of 0.61±0.01 $nm^2$ (i.e. consistent with what was reported for a 5.3:1 POPE to POPG system simulated by CHARMM36 force field[35]) to 0.85 $nm^2$. The extent of increase following each titration decreased as the bilayer approached butanol saturation (Fig. 2c, Table 1). At intercalated butanol:lipid ratios above 2:1 (BOL3-5) or butanol concentration higher than 2.0 *v/v* % (BOL2-10), bilayer disintegration was observed (Fig. 2d). However, at preceding sub-critical stages, (BOL2-9 and BOL3-4), the bilayer structure was well maintained even after 500-ns simulation time. The disintegration of the lipid bilayer is illustrated in terms of the gradual reduction in the area per lipid for simulations beyond the critical intercalated butanol:lipid ratio of 2:1 (Fig. S3b), as well as the transition of structure from normal bilayer (i), to buckled (ii) and finally completely disordered (iii) at butanol concentrations above the critical ratio (i.e. BOL3-5 in Fig. 2d).

Our data therefore show an upper limit of butanol that can be accommodated in the membrane to be close to 2:1 butanol:lipid ratio. Under moderate butanol concentrations (< 2.0 *v/v%*), the lipid

bilayer is stable with a dynamic balance between inside and outside butanol concentrations. Once beyond the ultimate adsorption capacity of the lipid bilayer (i.e. two butanols per phospholipid), the bilayer structure will be compromised.

**Butanol induces thinning of the bilayer, but not to the extent suggested by the fully interdigitation model**

In the absence of butanol, the density peaks of phosphorus atoms are sharp and spaced around 4 nm apart (Fig. 3a). The acyl tails of each leaflet show slight overlap and the total density profile of the system show an additional, distinct central minimum, consistent with the low-density midplane region between the two leaflets. As expected, the distribution of phosphorus (P) atoms overlaps with that of the water molecules, indicating that only the polar head region of the phospholipids is solvated, and that no water is entering the hydrophobic tail region, confirming that a stable semi-permeable lipid bilayer is formed. When butanol is added into the system, the total density profile of the system is flattened, with the disappearance of the central minimum observed for bilayer without butanol due to the larger overlap between the acyl chains from opposing leaflets (Fig. 3b-c). In parallel, there is a flattening and broadening of the P-atom peaks, likely due to larger bilayer fluctuations at high sub-critical butanol concentrations. Additionally, the P-atom peaks move closer together indicating that the bilayer is thinning. These results appear to be consistent with the model for lipid chain interdigitation[36].

To further investigate the apparent thinning effect, a 2D-thickness map[37] was constructed. Without butanol the membrane has a thickness of about 4.0 ± 0.3 nm (Fig. 4a), consistent with the density profile of P-atom as well as the value previously reported using a CHARMM force field[35]. The topology of the membrane became more undulated with each butanol titration (Fig. 4b-e) and at a sub-critical butanol concentration (i.e. BOL3-4 with butanol:lipid of about 1.9:1), the average membrane thickness had been reduced to about 3.38 ± 0.62 nm and only a minor portion of the membrane topology showed a thickness reduction of about 50%, to about 2-2.5 nm. Assuming a length of ~0.08 nm for a $CH_2$ unit[14], we estimate that a fully interdigitated system will experience a reduction in thickness of at least 1.5 nm (a ~1.14 nm reduction in the thickness was observed for a pure DMPC bilayer[38]). However, an appreciable drop in thickness in our modeling (Fig. 4f) is still much less than what would be expected, indicating that at sub-critical butanol concentration, POPE:POPG bilayer is likely not in a fully interdigitated state. This is noted that ~~further supported by~~ the simulation temperature~~, which~~ is ~~much~~ higher than the $T_m$ of both POPG and POPE (for comparison, the DMPC experiments were carried out at a temperature (~27°C) slightly above the $T_m$ (23°C) of DMPC), which renders the bilayer in a more disordered state. Moreover, unsaturated PE lipids is known to exhibit lower propensity to

adopt interdigitated structure. Whereas interdigitation would represent an increasingly ordered state, our modeling indicated that butanol had the opposite effect. Thus, the model of interdigitation by butanol needs to be revised or an alternative model should ~~to~~ be considered.

**Butanol increases bilayer disorder rather than induces an ordered gel state**

We further characterized the fluidity and mechanical property of the lipid bilayer with excess butanol in the bulk phase. The membrane partitioning of butanol markedly increased the lateral diffusion of lipids, as shown by an up to 3-4 fold increase in their diffusion coefficients (15-20 $\mu m^2/s$ compared to 5 $\mu m^2/s$ in the membrane system without butanol) as butanol:phospholipid ratios approaching the critical point (Fig. 5). The increase in fluidity was consistent with a modest increase in lateral diffusivity (from 2.2 to 2.8 $\mu m^2/s$ for 1 *v/v*% butanol) obtained by fluorescence recovery after photobleaching (FRAP) measurements of supported lipid bilayer on glass substrate (Fig. S4).

Additionally, the bending modulus ($K_c$) was estimated by our *in silico* approach to be reduced from ~$8.8\times10^{-20}$ J to ~$2.8\times10^{-20}$ J and ~$1.3\times10^{-20}$ J at butanol concentrations of 0.65% and 1.60 *v/v* %, respectively. This decrease in bending modulus was consistent with studies on giant unilamellar vesicles of SOPC and SOPS (99.5:0.5 mol %)[39], where a 50% reduction from ~$8\times10^{-20}$ J to ~ $4\times10^{-20}$ J was observed at 0.55 M butanol concentration. Considering the dramatic fluctuations of phospholipid observed at high butanol concentrations (Fig. 3b), the results indicate that the inclusion of butanol produces a more flexible membrane, in contrast with the gel-state predicted for interdigitation.

Finally, to evaluate the effects of butanol on lipid tails, the angular distributions of acyl chains with respect to the unperturbed membrane were determined to describe their orientations upon butanol exposure (Figs. 6a and S5a,b). In the absence of butanol, the most prevailing angles for *sn*-1 and *sn*-2 chains relative to membrane normal are around 23º and 157º. Butanol increases the tilt angle of the hydrocarbon chains, with tails adopting a more flat or splayed conformation (Fig. 6a). Moreover, their broader angle distribution indicates that lipid tails become more disordered with the increase of butanol concentration. Calculation of lipid order parameter, $S_{CD}$, further supports the increased disorder of phospholipids (Figs. 6b,c and S5c-f). According to the prevailing model for interdigitation, in order for the acyl tails from one leaflet to settle into the voids created by the assimilation of butanol in the other leaflet the acyl tails need to remain almost perpendicular to the bilayer interface. Our results thus strongly suggest that butanol decreases lipid order, which is manifested in membrane fluctuations and lateral mobility.

**Butanol accumulates non-uniformly and preferentially with the phospholipid heads**

In order to understand why our modelling predicts a critical butanol:lipid ratio of 2:1 (i.e. consistent with interdigitation[28, 40] yet fails to simulate the extent of thinning and increased order that would be expected from a fully interdigitated state, we considered further the averaged position of the butanol relative to the phospholipid. The model shows alignment of the butanol density peaks with those of the phosphorus atoms, suggesting, therefore, that butanol molecules are distributed non-uniformly throughout the bilayer, associating preferentially with the polar head groups of phospholipids (Fig. 3b). This is consistent with what has been described for the location of alcohols in lipid bilayers from NMR experiments[41, 42] and MD simulations[43]. The non-zero density of butanol at the vanishing midplane of the bilayer suggested by the molecular density profile (Fig. 3b) is more likely due to large bilayer fluctuations induced heterogeneity at the higher butanol concentration.

To further elucidate interactions between butanol and phospholipids, an atom-atom contact map with a 4.5 Å cutoff distance between the heavy atoms of butanol and POPE/POPG lipids was determined. At both low (i.e. 0.37 *v/v* %, Fig. 7a,b) and high (i.e. 1.99 *v/v* %, Fig. 7c,d) butanol concentrations, further evidence was provided of the greater tendency of butanol to interact with the phospholipid head groups through its polar terminus. Interactions between O and C1 atoms in butanol are almost exclusively with acyl chain atoms near the inter-molecular H-bond sites (i.e. the interfacial region) rather than the terminal acyl chains, demonstrating that the polar moiety of butanol does not penetrate deep within the hydrophobic core of the bilayer or between the leaflets. Furthermore, the methyl carbon atom of butanol mainly contacts with the carbon atoms in lipid tails near to the oxygen atoms of the carboxyl groups hydrogen-bonding with the hydroxyl in butanol. At sub-critical butanol concentration (i.e. butanol:lipid 1.9:1, Fig. 7c,d), the incidence of contacts between the last carbon atom of butanol and the lipid terminal methyls was observed. The intensities were much lower, however, than that suggested by a fully interdigitation model (Fig. 8a).

Butanol and POPE/POPG lipids are amphiphilic and their associations require both polar and hydrophobic interactions. However, as indicated by the contact map there is a discrepancy between alcohol polar associations to the phospholipid head group and hydrophobic pairings with their tails. This discrepancy is exacerbated in system that more accurately describes what takes place in a real system, where penetration into the bilayer is unidirectional. As illustrated by

Fig. S6, there is a delay in butanol transfer from the phospholipid head group of one leaflet to that of the other when butanol ingress is restricted to one leaflet only.

Butanol is therefore located at the interfacial region of the phospholipid and follows the same orientations as the lipids, with the polar head groups facing outwards to the solvent and the hydrophobic hydrocarbon tails pointing inwards. This lends support to the notion that bilayer fluctuation likely contributes to the non-zero density of butanol at the interleaflet space.

**Non-uniform accumulation of butanol around the phospholipid head leads to bilayer disorder**

The consequence of the accumulation of butanol molecules near the phospholipid polar head groups is that a hydrophobic void is created and that there is an unpaired butanol methyl group in the midst of the bilayer. As full penetration of butanol into the void is negligible (Fig. 7c,d), options for complementation of the unpaired butanol methyl are either interdigitation or bilayer disorder. Although the density distribution profiles and contact maps suggest the presence of an interdigitated phase, many other observations provided by MD simulations could also be interpreted as a highly disordered membrane.

As illustrated by the structures of some representative lipids (Fig. 8b-d), butanol molecules assemble around the lipid head groups either by hydrogen bonds directly or mediated through water molecules. The accumulation of butanol by the phospholipid head groups creates a lateral pressure gradient. While some lipids from the two leaflets are interdigitated with each other, a majority of the acyl chains deform to fill the voids between them, adopting a more flat or splayed conformation with large tilt angles (Fig. 6). Together, this leads to a general increase in disorder. In other word, butanol methyl groups looking to complex with other hydrophobic entities can thus do so with methyl groups of acyl tails from across the bilayer, but also with those from the same leaflet.

**Butanol-intercalated PE/PG mixed bilayer is sensitive to temperature**

The accumulation of small and rigid butanol at the interfacial region of phospholipids increases the space available for the fatty acid tails and causes them to form kinks (Fig. 7 and 8b-d). This disrupts the tight packing of the bilayer, leading to a reduced lipid ordering and an increased membrane fluidity (Fig. 5-6,S4). Longer fatty acids with larger acyl chain surface area generally result in stronger Van der Waals interactions and tighter lipid packing, which in turn requires

more energy inputs for a cooperative phase transition to occurs, characterized by $T_m$. Butanol reduces the $T_m$ of PE:PG bilayer (Fig. 1a).

To examine if the resultant disordered state of lipids, is more susceptible to temperature hikes, we further performed simulations at butanol concentrations of 1.60 and 1.99 *v/v* % at two higher temperatures, 320 K and 330 K. In our original simulations at 310 K, the bilayer structure at 1.99 *v/v* % was stable, but it was lost within 400 ns at both 320 K and 330 K. In comparison, the system at 1.60 *v/v* % showed high stability during 600 ns simulation time at both 320 K and 330 K. This suggests that the sensitivity (i.e. structural integrity) of PE/PG bilayer changes as a function of the butanol:lipid ratio. The more butanol in the bilayer, the more unstable the bilayer at higher temperature, consistent with the butanol's effect in lowering the phase transition temperature (Fig. 1a). Indeed, a reduction in the main transition temperature of the membrane system with increasing butanol concentration (two molecules per DMPC phospholipid) has been described[38].

It can be concluded that the liquid disordered POPE/POPG bilayer in the presence butanol is characterized by an irregular packing of lipids and butanol molecules, as well as acyl chain bending and splaying. This disordering stems from the non-complementary lengths of butanol and lipids, which effectively reduces the surface area of lipids accessible to neighbouring lipid molecules, weakens Van der Waals interactions, increases lipid fluidity and collectively contributes to a lowering of the main transition temperature.

**Molecular mechanism involved in butanol tolerance of *E*. coli inner membrane**

Based on the observations described herein (summarized in Fig. 9a), we propose a molecular mechanism for the effect of butanol on a bacterial inner membrane (Fig. 9b). First, when butanol is added to the *E. coli*, it accumulates around the phospholipid interfacial region and causes the headgroup region of membrane to expand, leading to packing defects and the appearance of voids between lipid chains. Such voids allow for the lipid tails of phospholipids within the same leaflet to bend and splay, which leads to disorder and membrane instability. These voids are also filled when the unpaired methyl of the butanol is complemented by the terminal acyl of disordered phospholipids from the opposing leaflet (i.e. partial interdigitation). Thus, upon butanol partitioning, the bilayer is short-circuited from two coupled leaflets into a single leaflet layer characterized by a continuous hydrophobic region, as supported by the density distribution profiles of the acyl chains and the reduced thickness of the bilayer.

While the critical butanol:lipid ratio of 2:1 satisfies the proposed interdigitated model, the inherent disorder caused by the monounsaturated phospholipids likely inhibit preferential hydrophobic pairing in an ordered fashion by interdigitation across the bilayer even in the presence of non-uniform accumulation of butanol at the head groups. While the reduction in bilayer thickness is not to the extent that would be expected for an interdigitated state, it might be nonetheless large enough to affect the diffusion of ions across the bilayer or influence the activity of membrane proteins. The function of cellular membranes also relies on their molecular order imparted by lipids.

Given that we have described the mechanism for membrane perturbation by butanol, it is interesting therefore to ruminate on strategies for arresting the butanol effect. In nature, for example, hopanoids have been suggested to reinforce bacterial membranes and protect against unfavourable environmental conditions like sterols in eukaryotes by modulating lipid order [44, 45]. It is possible, therefore, that hopanoids may arrest this degeneration into bilayer disorder and chaos and allow for complementation of the unpaired methyl group of butanol to occur in a less disruptive fashion. Thus, it may be possible to replicate this effect by means of exogenous membrane insertion molecules to enhance bilayer integrity and impede bilayer fluidization under high butanol concentrations. These findings implicate the potential of these molecules as targets to fight butanol toxicity and improve growth rates of bacteria in the presence of butanol[26].

## Conclusion

Here, we present a complete picture of the molecular responses of the inner membrane of *E. coli* to butanol. Firstly, there is a quick and dynamic partitioning of butanol into the bilayer. Butanol stress has components common to stress responses of other small organic molecules, such as preferring polar headgroups and outer edge of the hydrocarbon region. Then, an expansion of the lipid bilayer is observed due to the insertion of butanol, as well as the high fluidization and disorder induced by sacrificing the tight packing in the butanol-lipid hybrid membrane. Finally, the bilayer was collapsed and turned from two coupled leaflets into one accompanied by a drop in the membrane thickness. Furthermore, some key factors involved in butanol toxicity to cell membrane were identified, such as butanol concentration and temperature, providing an effective molecular model for the rational design of membrane insertion molecules to fortify microbial cell membranes. Cellular engineering based on these cues focused on inner membrane may assist in developing butanol tolerance butanol-producing host in the future. In order to elucidate the mechanism of biofuel molecules at atomic scale and to distinguish between their indirect effects via changes in membranes and their direct effects upon binding to membrane proteins, future

work will require the study of potential targets for biofuel molecules like porins embedded in explicit multicomponent membranes.

## Methods

### Large Unilamellar Vesicle (LUV) Preparation

POPE and POPG in chloroform solution were obtained from Avanti Polar Lipids, mixed to a molar ratio of 85:15 and dried under a gentle stream of nitrogen. The dried lipid was further desiccated overnight to obtain a thin lipid film. Rehydration of the dried film was carried out by adding Tris-NaCl buffer (25 mM Tris, 150 mM NaCl, pH = 7.5), to a concentration of 5 mg $mL^{-1}$, followed by incubation at 45 °C for 2 hours, under constant stirring using a magnetic stirrer at around 300 rpm. The sample was extruded 21 times through a 100 nm membrane and was kept at 4 °C until further use.

### Differential Scanning Calorimetry (DSC)

Calorimetric measurements were performed on Nano DSC differential scanning calorimeter (TA Instruments, New Castle, DE, USA). By applying a heating and cooling scan rate of 1˚C/min, thermograms from 5-35˚C were acquired for 1 mg/ml POPE:POPG LUVs. For butanol-containing samples, butanol was added prior to performing the measurement. Heating and cooling scans were repeated three times for each sample. The main transition temperature (Tm) is taken as the temperature of maximum heat capacity and the $\Delta H$ and $\Delta T_{1/2}$ were calculated, after baseline adjustment and normalization, using TA's NanoAnalyze v3.8.0 software.

### Simulations setup

The lipid bilayer were conducted using CHARMM-GUI Membrane Builder. [46-49] with 360 lipids (PE:PG=85:15), and three butanol concentrations varied from 1.8 to 5.4 % (*v/v*) were considered referred to hereafter as BOL1, BOL2 and BOL3 with150 mM NaCl. To mimic titration experiments where the bulk concentration of butanol is kept fixed, additional butanol molecules were added into each simulation system to maintain a particular number of free butanol molecules (100, 140 and 220, respectively) until no extra butanol molecules were adsorbed or the bilayer structure destroyed. Finally, a number of iterations for correcting the butanol concentration were performed, and BOL1, BOL2 and BOL3 have been simulated for 15, 10 and 5 stages, respectively. As a reference, a MD simulation of a butanol-free POPE/POPG lipid bilayer was simulated for 200 ns.

### Simulation details

All simulations were performed with GROMACS 5.1.2[50]. The united-atom force field parameters for POPE and POPG lipids were downloaded from lipidbook.bioch.ox.ac.uk.[51, 52] The

SPC water model[53] and periodic boundary conditions were used. In this work, all equilibration and production runs also followed the CHARMM-GUI Membrane Builder procedure. The systems were firstly minimized, and then equilibrated by gradually reducing restraint forces. At the beginning of equilibration, the time step was set to 1 fs, and then was changed to 2 fs. To ensure the successful equilibration, the NVT dynamics with constant volume and temperature was used for the first and second steps, and the NPT dynamics with constant temperature and pressure was applied for the rest equilibration steps and the production runs. The temperature was coupled with a Berendsen-thermostat to 310 K, the optimum temperature for *E. coli* growth[54], which is above the main phase transition temperature for pure POPE (26.1°C[55]) and pure POPG (–4°C[20]) bilayers, with a 1-ps time constant. The temperatures of the lipids and solvent were controlled independently. The pressure was maintained at 1 bar by using semiisotropic pressure coupling with the Parrinello-Rhaman barostat, and the time constant for coupling is 5 ps. The Particle-Mesh Ewald (PME) algorithm was used to treat long-range electrostatic interactions with a 1.2-nm cutoff distance. For Van der Waals interactions, the forces were smoothly switched to zero between twin range cut-offs at 1.0 and 1.2 nm. The neighbor list was updated every 20 steps during the simulations. All bonds with H-atoms were constrained using the LINCS algorithm.

The unidirectional butanol penetration into the bilayer were performed by applying an upper wall to the butanol molecules using the PLUMED plugin[56] to prevent them from interacting with the other bilayer leaflet.

**Simulation analysis**

The GridMAT-MD[37] package was used to analyse the bilayer thickness by measuring the distance of the phosphate groups in the upper and lower leaflets. The deuterium order parameter, lateral diffusion coefficients was calculated by the GROMACS software package[50]. The area compressibility modulus of the membrane ($K_A$) and bending modulus ($K_C$) were calculated according to references[57, 58]. The details of analysis techniques are provided as supplementary information.

**Mobility calculation by FRAP**

Fluorescence recovery after photobleaching (FRAP) technique was performed to derive the diffusion coefficient of the POPE:POPG (85:15) bilayer that has formed on the coverslip substrate. For obtaining fluorescence images, an inverted epifluorescence Eclipse TE 2000 microscope (Nikon, Tokyo, Japan) equipped with a 60 oil immersion objective (NA 1.49) and an Andor iXon + EMCCD camera (Andor Technology, Belfast, Northern iIreand) camera is used. The sample was illuminated through the TRITC (Rhodamine-DHPE) filter set with a mercury lamp (Intensilight C-HGFIE; Nikon Corporation). Before measuring the diffusivity by the FRAP experiments, the Solvent- Assisted Lipid Bilayer (SALB) was employed for the bilayer

formation procedure. To compare the time-lapsed influence of the butanol to the PE:PG bilayer, the FRAP was performed in three different experiment condition, before injection of butanol, 15 min after injection of the butanol and 1 hour after. The size of the bleaching circular spot is around 30 um diameter, and photobleached by 532 nm, 100 mW power of laser beam. The image traces of the recovery process were recorded from minus 3 to 120 sec at two seconds of interval time to monitor the recovery process of fluorescence intensity signal. FRAP analysis was computed using Matlab software in order to acquire the diffusion coefficients that are determined based on the Hankel transform method.

## References


1. Atsumi S., *et al.* Metabolic engineering of Escherichia coli for 1-butanol production. *Metab. Eng.* **10**, 305-311 (2008).
2. Chin W.-C., Lin K.-H., Chang J.-J., Huang C.-C. Improvement of n-butanol tolerance in Escherichia coli by membrane-targeted tilapia metallothionein. *Biotechnol. Biofuels* **6**, 130 (2013).
3. Lee J. Y., Yang K. S., Jang S. A., Sung B. H., Kim S. C. Engineering butanol-tolerance in Escherichia coli with artificial transcription factor libraries. *Biotechnol. Bioeng.* **108**, 742-749 (2011).
4. Ingram L. O. Adaptation of membrane lipids to alcohols. *J. Bacteriol.* **125**, 670-678 (1976).
5. Bowles L. K., Ellefson W. L. Effects of butanol on Clostridium acetobutylicum. *Appl. Environ. Microbiol.* **50**, 1165-1170 (1985).
6. Ezeji T., Milne C., Price N. D., Blaschek H. P. Achievements and perspectives to overcome the poor solvent resistance in acetone and butanol-producing microorganisms. *Appl. Microbiol. Biotechnol.* **85**, 1697-1712 (2010).
7. Vollherbst-Schneck K., Sands J. A., Montenecourt B. S. Effect of butanol on lipid composition and fluidity of Clostridium acetobutylicum ATCC 824. *Appl. Environ. Microbiol.* **47**, 193-194 (1984).
8. Baer S. H., Blaschek H. P., Smith T. L. Effect of butanol challenge and temperature on lipid composition and membrane fluidity of butanol-tolerant Clostridium acetobutylicum. *Appl. Environ. Microbiol.* **53**, 2854-2861 (1987).
9. Nambi P., Rowe E. S., McIntosh T. J. Studies of the ethanol-induced interdigitated gel phase in phosphatidylcholines using the fluorophore 1, 6-diphenyl-1, 3, 5-hexatriene. *Biochemistry (Mosc.)* **27**, 9175-9182 (1988).
10. Zhang F., Rowe E. S. Titration calorimetric and differential scanning calorimetric studies of the interactions of n-butanol with several phases of dipalmitoylphosphatidylcholine. *Biochemistry (Mosc.)* **31**, 2005-2011 (1992).
11. Li S., Lin H., Wang G., Huang C. Effects of alcohols on the phase transition temperatures of mixed-chain phosphatidylcholines. *Biophys. J.* **70**, 2784-2794 (1996).
12. Huang C., McIntosh T. J. Probing the ethanol-induced chain interdigitations in gel-state bilayers of mixed-chain phosphatidylcholines. *Biophys. J.* **72**, 2702-2709 (1997).
13. Rowe E. S., Campion J. M. Alcohol induction of interdigitation in distearoylphosphatidylcholine: fluorescence studies of alcohol chain length requirements. *Biophys. J.* **67**, 1888-1895 (1994).
14. Adachi T., Takahashi H., Ohki K., Hatta I. Interdigitated structure of phospholipid-alcohol systems studied by x-ray diffraction. *Biophys. J.* **68**, 1850-1855 (1995).

15. Toppozini L., *et al.* Partitioning of ethanol into lipid membranes and its effect on fluidity and permeability as seen by X-ray and neutron scattering. *Soft Matter* **8**, 11839 (2012).
16. Gurtovenko A. A., Anwar J. Interaction of Ethanol with Biological Membranes: The Formation of Non-bilayer Structures within the Membrane Interior and their Significance. *J. Phys. Chem. B* **113**, 1983-1992 (2009).
17. Griepernau B., Leis S., Schneider M. F., Sikor M., Steppich D., Böckmann R. A. 1-Alkanols and membranes: A story of attraction. *Biochim. Biophys. Acta* **1768**, 2899-2913 (2007).
18. Patra M., *et al.* Under the influence of alcohol: the effect of ethanol and methanol on lipid bilayers. *Biophys. J.* **90**, 1121-1135 (2006).
19. McIntosh T. J., Lin H., Li S., Huang C.-h. The effect of ethanol on the phase transition temperature and the phase structure of monounsaturated phosphatidylcholines. *Biochimica et Biophysica Acta (BBA)-Biomembranes* **1510**, 219-230 (2001).
20. Boggs J. M., Tümmler B. Interdigitated gel phase bilayers formed by unsaturated synthetic and bacterial glycerolipids in the presence of polymyxin B and glycerol. *Biochim. Biophys. Acta* **1145**, 42-50 (1993).
21. Sum A. K., Faller R., de Pablo J. J. Molecular simulation study of phospholipid bilayers and insights of the interactions with disaccharides. *Biophys. J.* **85**, 2830-2844 (2003).
22. Malajczuk C. J., Hughes Z. E., Mancera R. L. Molecular dynamics simulations of the interactions of DMSO, mono-and polyhydroxylated cryosolvents with a hydrated phospholipid bilayer. *Biochim. Biophys. Acta* **1828**, 2041-2055 (2013).
23. Posokhov Y. O., Kyrychenko A. Effect of acetone accumulation on structure and dynamics of lipid membranes studied by molecular dynamics simulations. *Comput. Biol. Chem.* **46**, 23-31 (2013).
24. Odinokov A., Ostroumov D. Structural Degradation and Swelling of Lipid Bilayer under the Action of Benzene. *J. Phys. Chem. B* **119**, 15006-15013 (2015).
25. Fabian B., Darvas M., Picaud S., Sega M., Jedlovszky P. The effect of anaesthetics on the properties of a lipid membrane in the biologically relevant phase: a computer simulation study. *Phys. Chem. Chem. Phys.* **17**, 14750-14760 (2015).
26. Hinks J., *et al.* Increased Microbial Butanol Tolerance by Exogenous Membrane Insertion Molecules. *ChemSusChem* **8**, 3718-3726 (2015).
27. Comer J., Schulten K., Chipot C. Permeability of a Fluid Lipid Bilayer to Short-Chain Alcohols from First Principles. *J. Chem. Theory Comput.* **13**, 2523-2532 (2017).
28. Kranenburg M., Vlaar M., Smit B. Simulating induced interdigitation in membranes. *Biophys. J.* **87**, 1596-1605 (2004).
29. Frischknecht A. L., Frink L. J. D. Alcohols reduce lateral membrane pressures: predictions from molecular theory. *Biophys. J.* **91**, 4081-4090 (2006).
30. Dickey A. N., Faller R. Investigating interactions of biomembranes and alcohols: A multiscale approach. *J. Polym. Sci., Part B: Polym. Phys.* **43**, 1025-1032 (2005).
31. Dickey A. N., Faller R. How alcohol chain-length and concentration modulate hydrogen bond formation in a lipid bilayer. *Biophys. J.* **92**, 2366-2376 (2007).
32. Murzyn K., Róg T., Pasenkiewicz-Gierula M. Phosphatidylethanolamine-Phosphatidylglycerol Bilayer as a Model of the Inner Bacterial Membrane. *Biophys. J.* **88**, 1091-1103 (2005).
33. Navas B. P., *et al.* Composition dependence of vesicle morphology and mixing properties in a bacterial model membrane system. *Biochimica et Biophysica Acta (BBA)-Biomembranes* **1716**, 40-48 (2005).
34. Garidel P., Blume A. Miscibility of phosphatidylethanolamine-phosphatidylglycerol mixtures as a function of pH and acyl chain length. *Eur. Biophys. J.* **28**, 629-638 (2000).
35. Pandit K. R., Klauda J. B. Membrane models of E. coli containing cyclic moieties in the aliphatic lipid chain. *Biochim. Biophys. Acta* **1818**, 1205-1210 (2012).
36. Lin X., Zhang S., Ding H., Levental I., Gorfe A. A. The aliphatic chain of cholesterol modulates bilayer interleaflet coupling and domain registration. *FEBS Lett.* **590**, 3368-3374 (2016).

37. Allen W. J., Lemkul J. A., Bevan D. R. GridMAT-MD: a grid-based membrane analysis tool for use with molecular dynamics. *J. Comput. Chem.* **30**, 1952-1958 (2009).
38. Rifici S., *et al.* Effects of a short length alcohol on the dimyristoylphosphatidylcholine system. *Philos. Mag.* **91**, 2014-2020 (2011).
39. Ly H. V., Longo M. L. The influence of short-chain alcohols on interfacial tension, mechanical properties, area/molecule, and permeability of fluid lipid bilayers. *Biophys. J.* **87**, 1013-1033 (2004).
40. Kranenburg M., Smit B. Simulating the effect of alcohol on the structure of a membrane. *FEBS Lett.* **568**, 15-18 (2004).
41. Feller S. E., Brown C. A., Nizza D. T., Gawrisch K. Nuclear overhauser enhancement spectroscopy cross-relaxation rates and ethanol distribution across membranes. *Biophys. J.* **82**, 1396-1404 (2002).
42. Holte L. L., Gawrisch K. Determining ethanol distribution in phospholipid multilayers with MAS-NOESY spectra. *Biochemistry (Mosc.)* **36**, 4669-4674 (1997).
43. Chanda J., Bandyopadhyay S. Perturbation of Phospholipid Bilayer Properties by Ethanol at a High Concentration. *Langmuir* **22**, 3775-3781 (2006).
44. Saenz J. P., *et al.* Hopanoids as functional analogues of cholesterol in bacterial membranes. *Proc. Natl. Acad. Sci. U. S. A.* **112**, 11971-11976 (2015).
45. Caron B., Mark A. E., Poger D. Some Like It Hot: The Effect of Sterols and Hopanoids on Lipid Ordering at High Temperature. *J Phys Chem Lett* **5**, 3953-3957 (2014).
46. Jo S., *et al.* Lipopolysaccharide membrane building and simulation. *Methods Mol. Biol.* **1273**, 391-406 (2015).
47. Jo S., Lim J. B., Klauda J. B., Im W. CHARMM-GUI Membrane Builder for mixed bilayers and its application to yeast membranes. *Biophys. J.* **97**, 50-58 (2009).
48. Jo S., Kim T., Im W. Automated builder and database of protein/membrane complexes for molecular dynamics simulations. *PLoS ONE* **2**, e880 (2007).
49. Wu E. L., *et al.* CHARMM-GUI Membrane Builder toward realistic biological membrane simulations. *J. Comput. Chem.* **35**, 1997-2004 (2014).
50. Van Der Spoel D., Lindahl E., Hess B., Groenhof G., Mark A. E., Berendsen H. J. GROMACS: fast, flexible, and free. *J. Comput. Chem.* **26**, 1701-1718 (2005).
51. Domański J., Stansfeld P. J., Sansom M. S., Beckstein O. Lipidbook: a public repository for force-field parameters used in membrane simulations. *J. Membr. Biol.* **236**, 255-258 (2010).
52. Piggot T. J., Holdbrook D. A., Khalid S. Electroporation of the E. coli and S. Aureus membranes: molecular dynamics simulations of complex bacterial membranes. *J. Phys. Chem. B* **115**, 13381-13388 (2011).
53. Berendsen H. J., Postma J. P., van Gunsteren W. F., Hermans J. Interaction models for water in relation to protein hydration. *Intermolecular forces*, 331-342 (1981).
54. Noor R., Islam Z., Munshi S. K., Rahman F. Influence of Temperature on Escherichia coli Growth in Different Culture Media. *Journal of Pure and Applied Microbiology* **7**, 899-904 (2013).
55. Wang Z.-q., Lin H., Li S., Huang C.-H. Calorimetric studies and molecular mechanics simulations of monounsaturated phosphatidylethanolamine bilayers. *J. Biol. Chem.* **269**, 23491-23499 (1994).
56. Tribello G. A., Bonomi M., Branduardi D., Camilloni C., Bussi G. PLUMED 2: New feathers for an old bird. *Comput. Phys. Commun.* **185**, 604-613 (2014).
57. Bochicchio D., Panizon E., Monticelli L., Rossi G. Interaction of hydrophobic polymers with model lipid bilayers. *Sci Rep* **7**, 6357 (2017).
58. Hu M., IV P. D., Deserno M. Determining the bending modulus of a lipid membrane by simulating buckling. *J. Chem. Phys.* **138**, (2013).

## Acknowledgements

The computational work for this article was performed on resources of the National Supercomputing Centre, Singapore (https://www.nscc.sg). This work was supported by Grant xxxxx.

## Author Contributions

J.G. carried out the MD simulations and analyses. Xxx carried out the experimental validation. J.G., Y.M. and T.M. designed the research and coordinated the study. XXX helped draft the manuscript.

## Competing Interests statement

The authors declare no competing financial interests.

# Tables

## Table 1.

System information of each system, including the number of water and butanol, and the average and standard deviation of butanol concentration in the bulk, butanol:lipid ratio and area per lipid during the 80-100 ns trajectory.

| | Num. (water) | | | Num. (butanol) | | | Butanol concentration (*v/v* %) | | | Butanol:Lipid ratio | | | Area per lipid (nm$^2$) | | |
|---|---|---|---|---|---|---|---|---|---|---|---|---|---|---|---|
| System | BOL1 | BOL2 | BOL3 | BOL1 | BOL2 | BOL3 | BOL1 | BOL2 | BOL3 | BOL1 | BOL2 | BOL3 | BOL1 | BOL2 | BOL3 |
| 1 | 19252 | 18924 | 18639 | 87 | 172 | 248 | 0.37±0.11 | 0.56±0.13 | 0.65±0.16 | 0.21±0.01 | 0.43±0.01 | 0.63±0.01 | 0.64±0.01 | 0.68±0.01 | 0.70±0.01 |
| 2 | 21585 | 19896 | 19270 | 176 | 279 | 453 | 0.59±0.11 | 0.77±0.14 | 1.16±0.26 | 0.43±0.01 | 0.70±0.01 | 1.15±0.02 | 0.67±0.01 | 0.72±0.01 | 0.79±0.01 |
| 3 | 22257 | 20136 | 20734 | 248 | 398 | 640 | 0.70±0.15 | 1.02±0.18 | 1.60±0.25 | 0.62±0.01 | 1.01±0.01 | 1.61±0.02 | 0.71±0.01 | 0.78±0.01 | 0.87±0.01 |
| 4 | 23998 | 27954 | 29010 | 308 | 502 | 810 | 1.00±0.14 | 1.37±0.17 | 1.99±0.19 | 0.74±0.01 | 1.20±0.02 | 1.93±0.03 | 0.72±0.01 | 0.81±0.01 | 0.85±0.01 |
| 5 | 24532 | 30113 | 30544 | 372 | 589 | 926 | 1.15±0.16 | 1.40±0.14 | 1.98±0.20 | 0.90±0.02 | 1.42±0.02 | 2.23±0.03 | 0.75±0.01 | 0.82±0.02 | 0.84±0.02 |
| 6 | 28817 | 32340 | / | 432 | 658 | / | 1.09±0.12 | 1.45±0.15 | / | 1.04±0.01 | 1.58±0.02 | / | 0.78±0.01 | 0.83±0.01 | / |
| 7 | 31854 | 32793 | / | 478 | 714 | / | 1.30±0.11 | 1.74±0.16 | / | 1.12±0.02 | 1.68±0.02 | / | 0.79±0.01 | 0.84±0.01 | / |
| 8 | 29940 | 32941 | / | 507 | 763 | / | 1.33±0.14 | 1.77±0.17 | / | 1.21±0.02 | 1.80±0.02 | / | 0.79±0.01 | 0.83±0.01 | / |
| 9 | 28957 | 33239 | / | 543 | 803 | / | 1.37±0.17 | 1.90±0.23 | / | 1.31±0.02 | 1.89±0.04 | / | 0.81±0.01 | 0.86±0.02 | / |
| 10 | 29550 | 36196 | / | 579 | 838 | / | 1.53±0.13 | 2.07±0.15 | / | 1.38±0.02 | 1.92±0.03 | / | 0.82±0.01 | 0.86±0.01 | / |
| 11 | 31080 | / | / | 607 | / | / | 1.49±0.13 | / | / | 1.44±0.02 | / | / | 0.81±0.02 | / | / |
| 12 | 32662 | / | / | 635 | / | / | 1.59±0.12 | / | / | 1.49±0.02 | / | / | 0.83±0.02 | / | / |
| 13 | 32625 | / | / | 669 | / | / | 1.57±0.16 | / | / | 1.59±0.02 | / | / | 0.84±0.02 | / | / |
| 14 | 32148 | / | / | 706 | / | / | 1.63±0.14 | / | / | 1.68±0.02 | / | / | 0.85±0.01 | / | / |
| 15 | 35043 | / | / | 713 | / | / | 1.67±0.18 | / | / | 1.67±0.03 | / | / | 0.85±0.01 | / | / |

**Table 2 The softening of membrane suggested by the bending modulus ($K_c$) of membranes at strain (γ) of 0.15.**

| System | γ | Butanol-free | BOL3-1 | BOL3-3 |
|---|---|---|---|---|
| $K_c$ ($10^{-20}$J) | 0.15 | 8.79 ± 0.01 | 2.78 ± 1.91 | 1.13 ± 2.06 |

## Figure Legends

**Fig. 1** Reduction of main transition temperature of membrane by butanol.

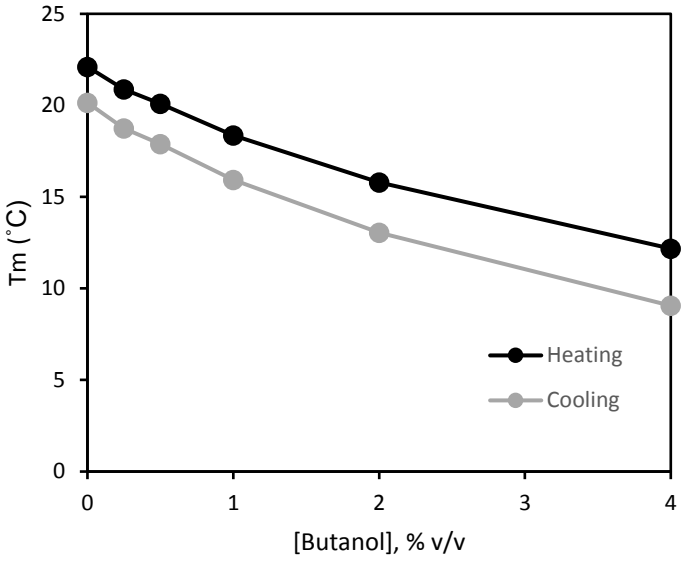

**Fig. 2** The partitioning of butanol into membrane. **a** A flowchart of the strategy used in our simulations. **b** Butanol partitioning of BOL3. The reference lines were calculated based on all butanol molecules in the simulation. For clarity, a windowed average over a period of 1 ns is shown. **c** Area per lipid of the butanol-free system and BOL3 along the first 100 ns. **d** Snapshots at different simulation time for BOL3-5. Solvent is shown as transparent surfaces, bilayers as lines with carbon atoms in gray, and butanol as green spheres.

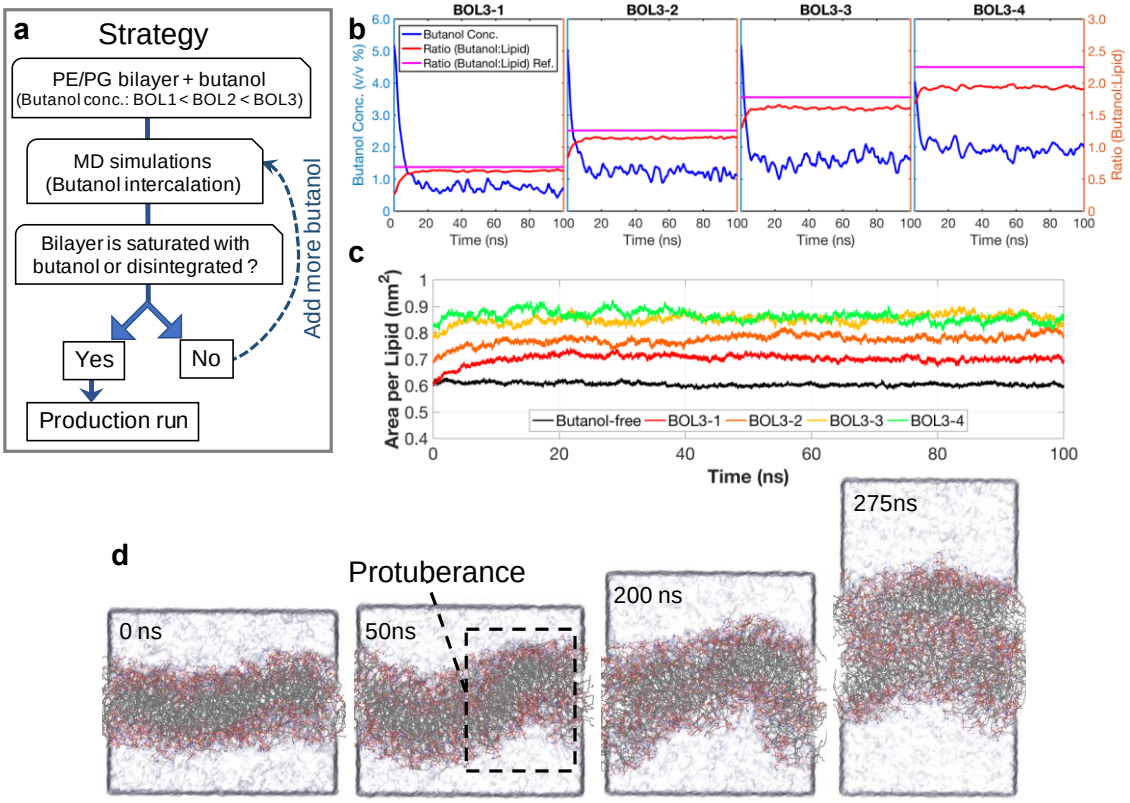

**Fig. 3** Density distribution profiles of selected chemical groups along the membrane normal axis during the last 20 ns: **a** butanol-free; **b** BOL3-3; **c** the overlap area between the density distribution profiles of the two tails between leaflets.

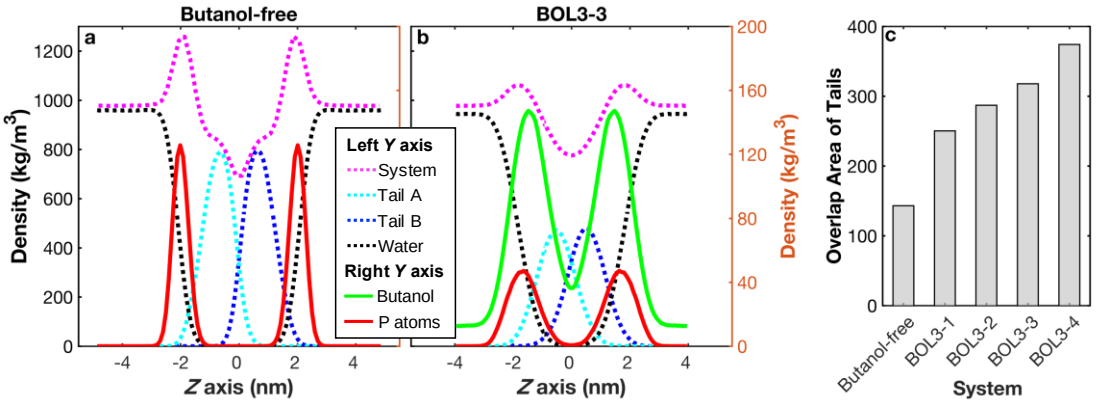


**Fig. 4** Membrane thickness. **a-e** Averaged 2D-membrane thickness map during the last 10 ns for the butanol-free systems and all systems of BOL3. **f** Averaged lipid bilayer thickness during 80-100 ns simulations for all systems.

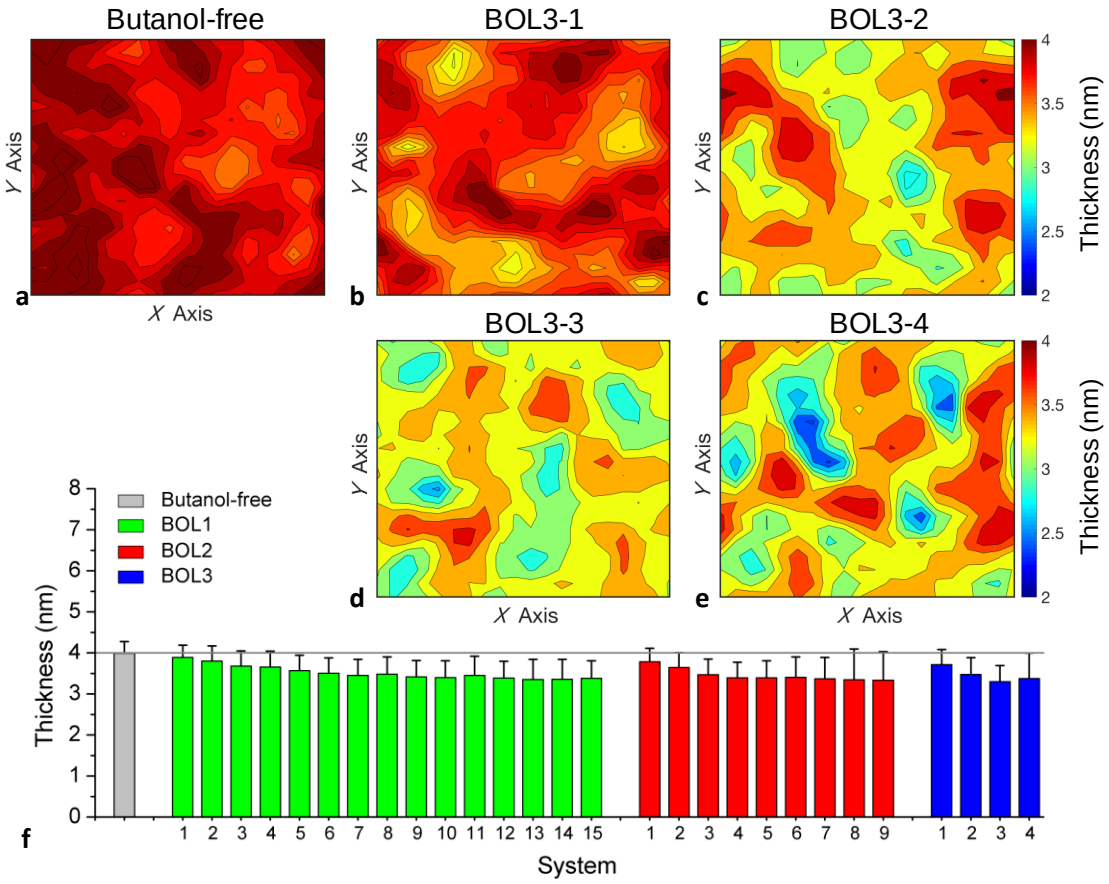

**Fig. 5** Lateral diffusion coefficients of lipids in the absence and presence of butanol.

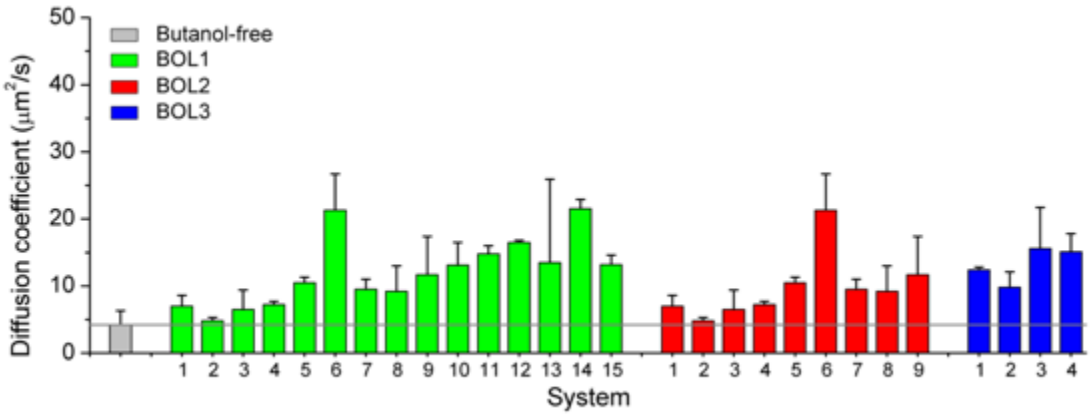


**Fig. 6** Orientation and ordering of lipid tails for BOL3 in compared with the butanol-free system. **a** Angular distributions of chain vectors from the first to the last carbon with respect to the outward bilayer normal. **b-c** The deuterium order parameters ($S_{CD}$) of the acyl chains.

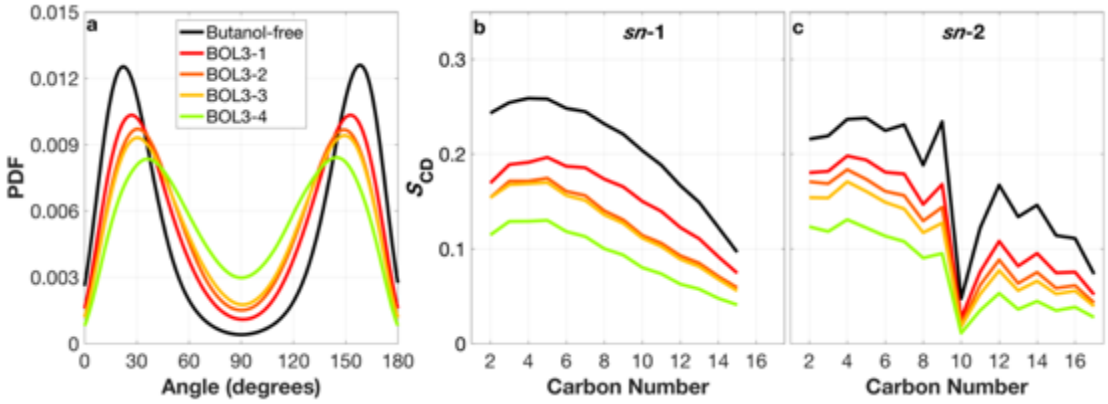

**Fig. 7** Atom-atom contact maps between the heavy atoms of butanol and POPE/POPG lipids: **a-b** BOL1-1 and **c-d** BOL3-4.

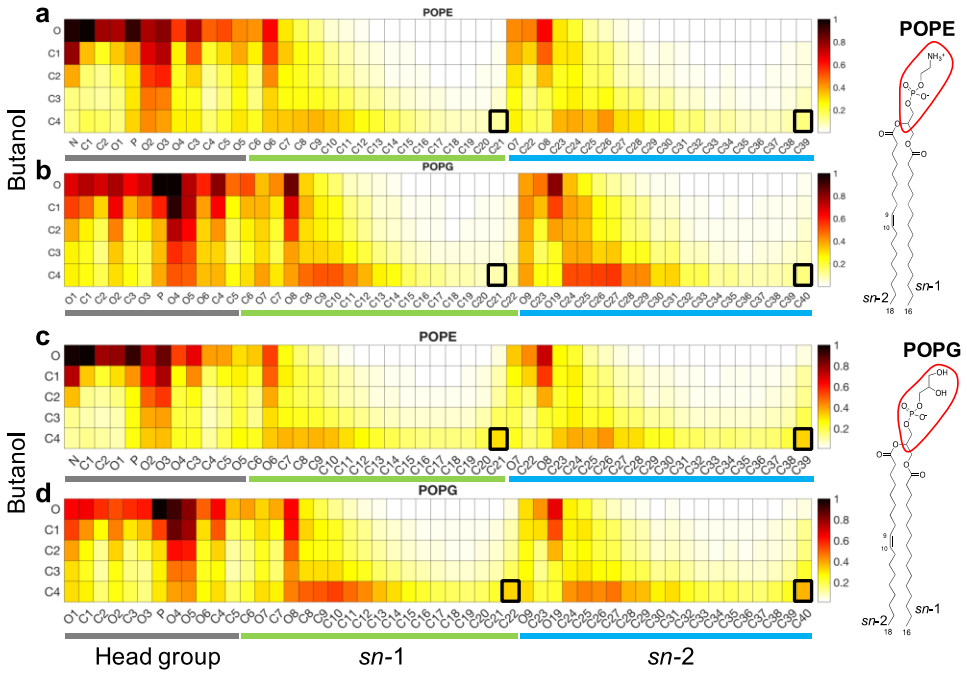


**Fig. 8** The diagram of lipid bilayer conformations in the presence of butanol. **a** The fully interdigitated membrane model. **b-d** The representative lipid conformation in the fluid phase with exposure to butanol. The solvent was shown as white transparent surface, lipids as gray lines, and phosphorus atoms as yellow spheres. For clarity, only part of lipids and phosphorus atoms were shown. The highlighted lipids were represented as cyan, green and purple sticks, butanol as orange sticks, and two water molecules as spheres. In the sketch map, the intermolecular hydrogen bonds were shown as purple dash lines among lipids, butanol and waters (red dots). Interdigitation and splaying of the acyl chains were highlighted.

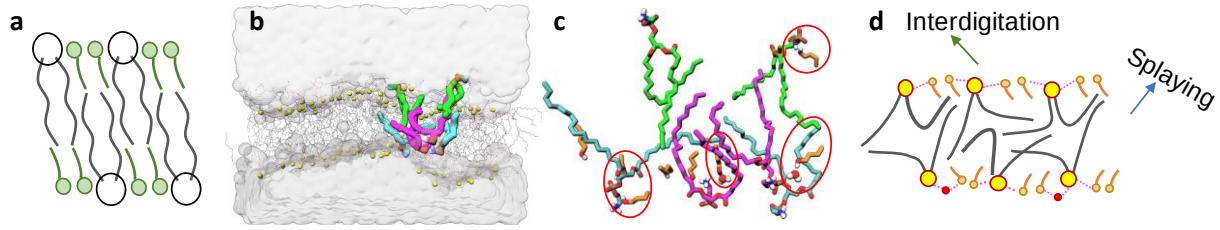

**Fig. 9** Molecular mechanism involved in butanol tolerance of *E. coli* inner membrane: **a** summary of butanol effects on lipid bilayer; **b** a schematic model illustrating of the molecular mechanism involved in butanol partitioning into the inner membrane of *E. coli*.

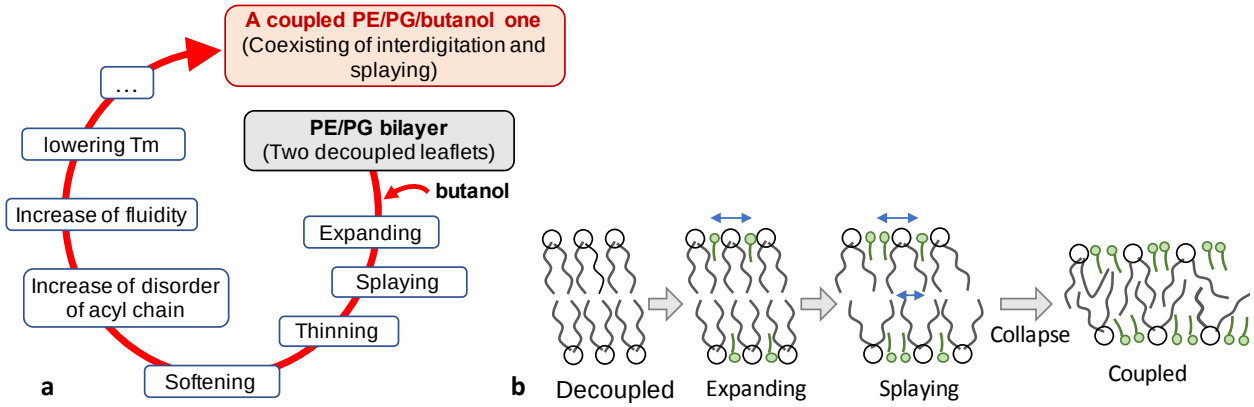

# Supplementary Information

## Simulation analysis

**Definition of intercalated and free butanol.** Butanol molecules are divided into three groups based on the minimum distance between a butanol and the membrane: a) intercalated butanol inside the membrane (< 4.5 Å); b) accumulated butanol layer around the membrane (>= 4.5 Å and <=7 Å); c) free butanol (> 7 Å). Then two parameters are defined: butanol (intercalated ones) to lipid ratio, and butanol concentration (*v/v*) in the bulk. The latter one is calculated based on the numbers of water and butanol molecules with the minimum distance from lipids larger than 7 Å.

**Area per lipid.** Here, we chose the conventional approach to calculate the area per lipid, in which the total area of the simulation box was divided by the number of lipids in one monolayer and the area of the butanol molecules was neglected. The calculation can be simply as:

$$< A_{lipid} > = \frac{2 < XY >}{N_{lipid}}$$

where $< A_{lipid} >$ is area per lipid, $< XY >$ is the area of simulation box, and $N_{lipid}$ is the number of lipids in the system.

**2D-thickness map.** GridMAT-MD was employed here to measure the effect of butanol on the membrane thickness. The phosphorous atoms in the lipid head group were served as the reference atom, upon which a grid was used to determine their locations and to calculate the local thicknesses. Total bilayer thicknesses were taken by averaging data from the last 20 ns every 200 ps.

**The angular distributions.** The orientations of the head group (P-N vector in POPE and P-C vector in POPG) and the angular distributions of the vectors between the first and last carbons of the hydrocarbon chains were calculated with respect to the bilayer.

**Deuterium order parameters.** The order parameter of lipid tails indicates the orientation of the carbon chain, which is calculated using GROMACS as the following equation:

$$S_z = \frac{3}{2} < cos^2\theta_z > - \frac{1}{2}$$

where $\theta_z$ is the angle between the *z*-axis of the simulation box (membrane normal) and the carbon−deuterium vector of the *i*th methylene group in the lipid tails. Order parameters vary between 1 and –0.5 indicating a fully order along the normal direction to a fully order perpendicular to the normal direction. In general, order decreases from the interface region to the bilayer center.

**Lateral diffusion coefficients.** GROMACS is used to measure the lateral diffusion coefficient of lipids, which is determined by linear regression of the mean square displacement (MSD) of the phosphorus atom of the headgroup based on the 80-100 ns trajectories. An error estimate is given to show the difference of the diffusion coefficients over the two halves of the fit interval (2-15 ns).

**Mechanical properties.** The membrane buckling method was chosen for the measurement of the membrane bending modulus $K_C$. Firstly, a buckled lipid bilayer was generated by using anisotropic pressure coupling, with a pressure of 6 bar in the *x* direction until a strain of 0.2 was achieved. Then, a 100-ns simulation was performed by fixing the box length in *x* and *y* directions, and the *xx* component of the stress tensor was used to derive the force exerted by the membrane in the *x* direction, which is related to $K_C$. The last 50 ns was used for analyses.

## Supplementary figures

**Fig. S1** The effects of butanol on main transition temperature of lipid bilayer.

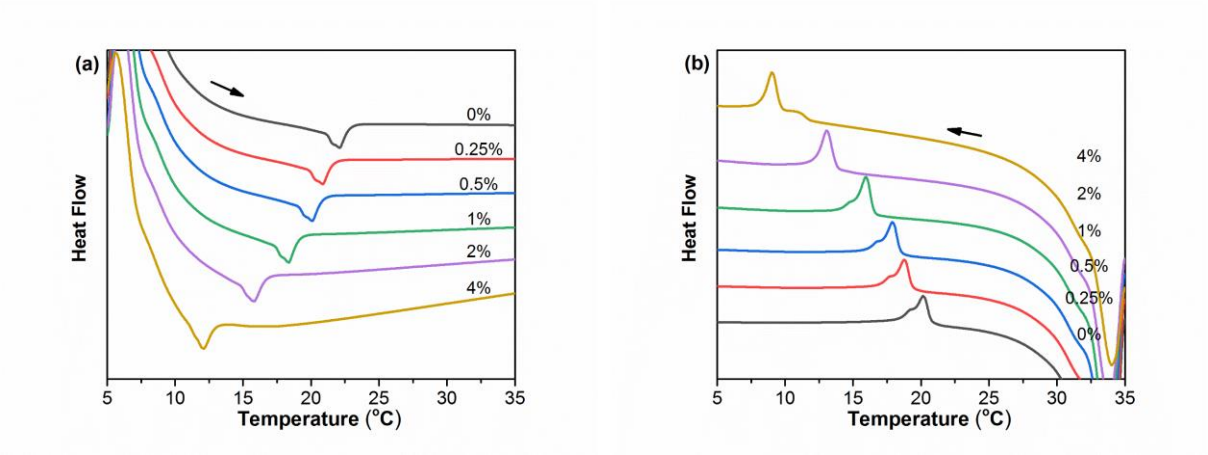


**(c)**

| Butanol (%) | Heating (°C) | Cooling (°C) | $\Delta T_m$ | $T_m$ Hysteresis |
|---|---|---|---|---|
| 0 | 22.11 | 20.15 | N.A. | - 1.96 |
| 0.25 | 20.88 | 18.77 | -1.23 | - 2.11 |
| 0.5 | 20.11 | 17.89 | -2.00 | -2.22 |
| 1 | 18.37 | 15.92 | -3.74 | -2.45 |
| 2 | 15.83 | 13.07 | -6.28 | -2.76 |
| 4 | 12.11 | 9.07 | -10.00 | -3.04 |

**(d)**

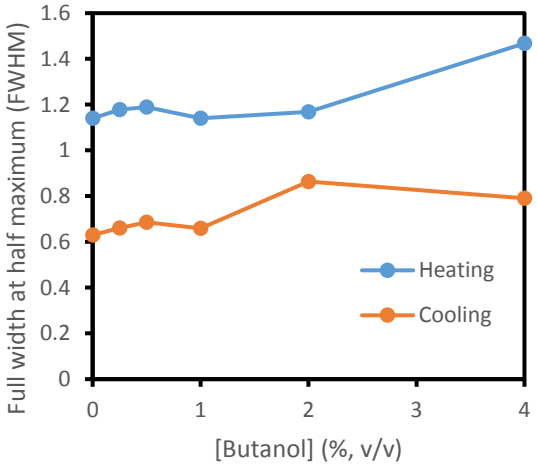

**Fig. S2** The partitioning of butanol into membrane. **a** Snapshots at different simulation time for BOL3-1. Solvent is shown as transparent surfaces, bilayers as lines with carbon atoms in gray, and butanol as green spheres. Dynamic balance between butanol inside the bilayer and in the bulk in the first stage of each system: **b** butanol to lipid ratio of each system along the simulation time (left panel) and the probability distribution profiles of last 50 ns; **c** butanol concentration (*v/v*) of each system along the simulation time (left panel) and the probability distribution profiles of last 50 ns.

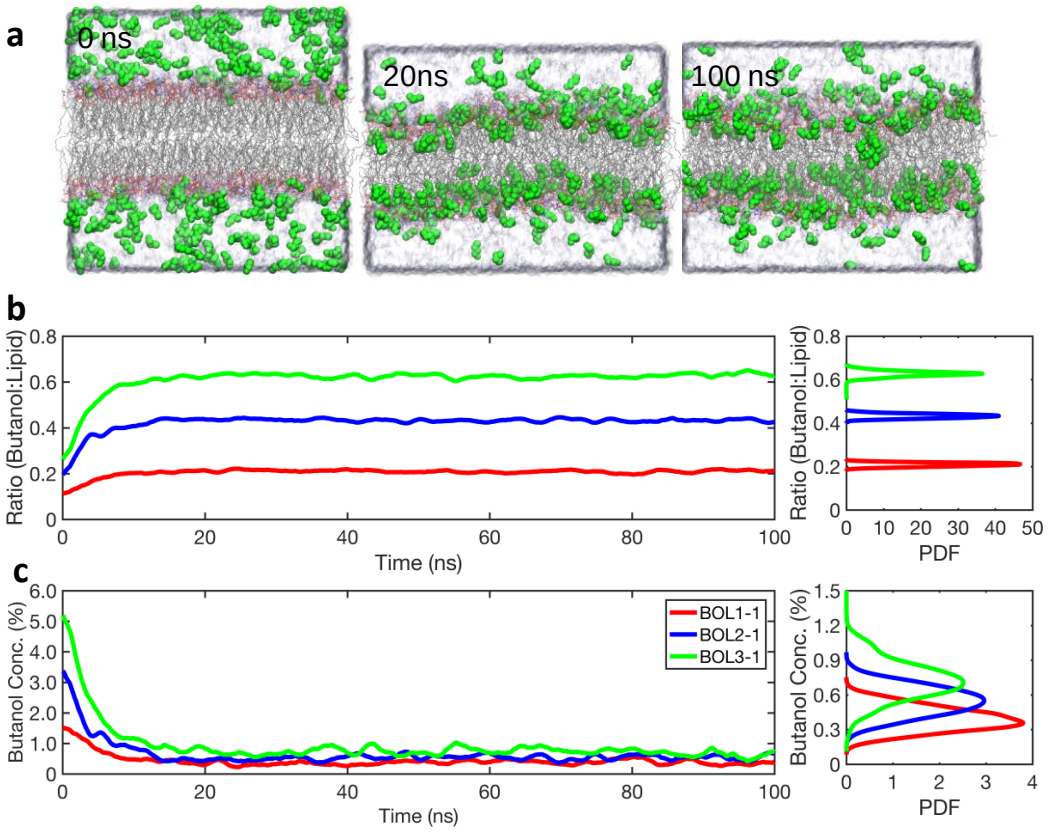

**Fig. S3** Comparison of area per lipid among all systems: **a** area per lipid of each system along the first 100 ns; **b** area per lipid along a longer simulation time. Related to Table 1.

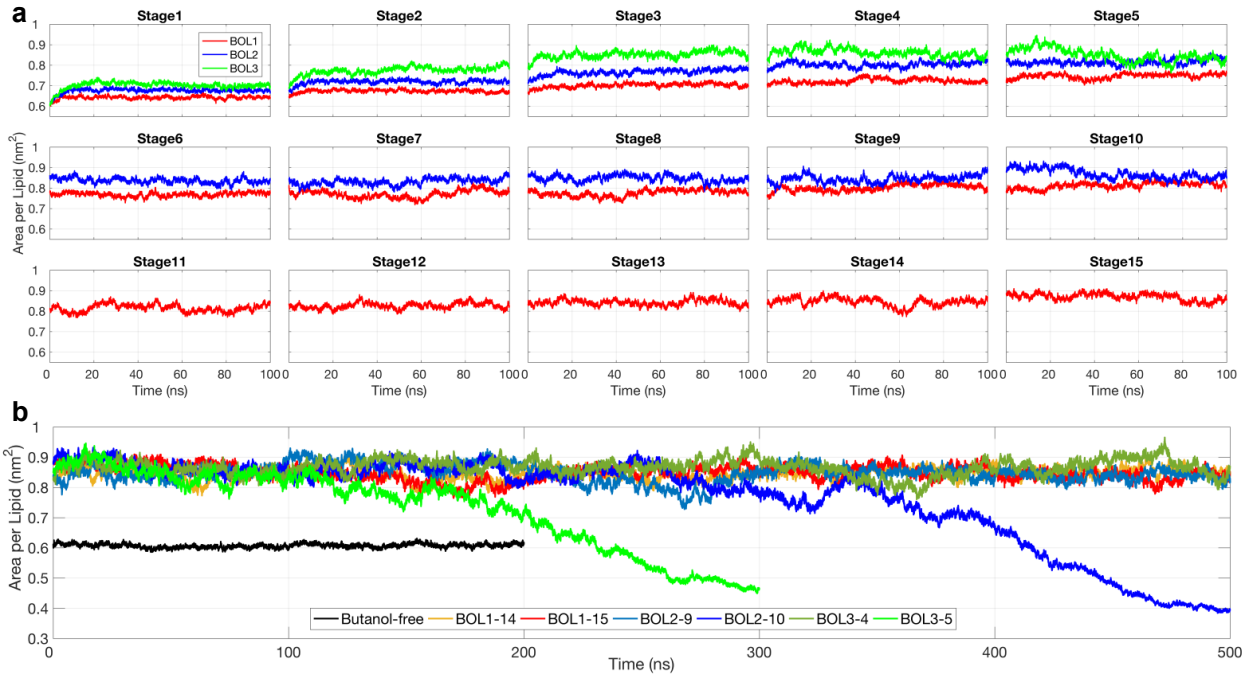


**Fig. S4** Fluorescence recovery after photobleaching (FRAP) measurement.

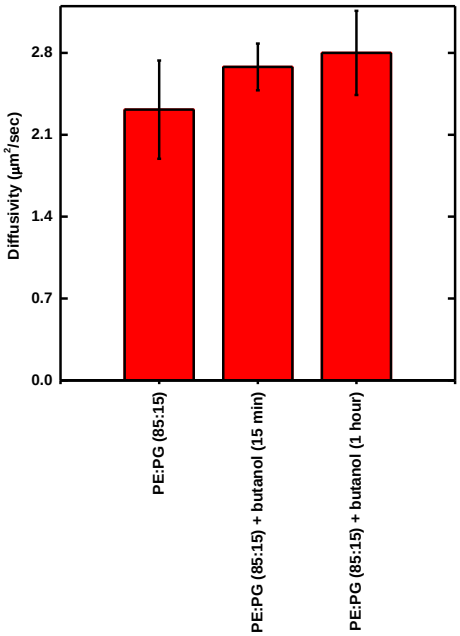

**Fig. S5** Orientation and ordering of lipid tails for BOL1 and BOL2 in compared with the butanol-free system. For caption, see Fig. 5.

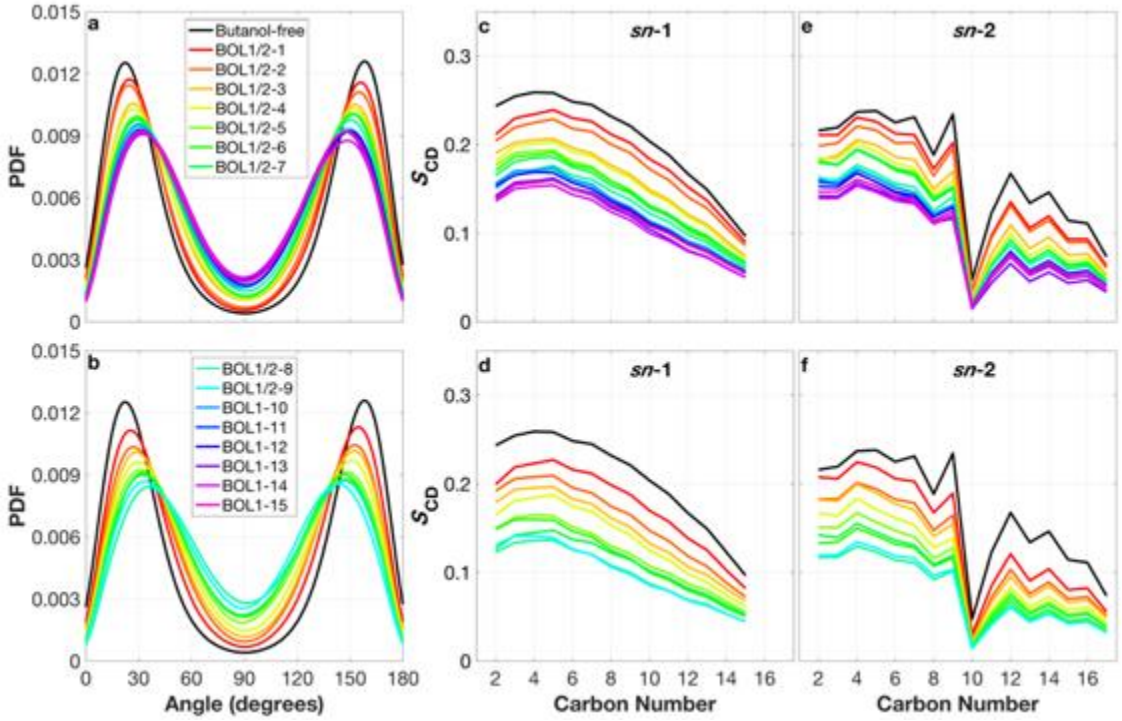


**Fig. S6** Unidirectional butanol penetration into the bilayer. Snapshots at 0 ns, 20 ns and 500 ns.